PCCP

PAPER

View Article Online
View Journal | View Issue

Cite this: *Phys. Chem. Chem. Phys.*, 2024, **26**, 24179

Photoisomerization pathways of *trans*-resveratrol†

Mariana Yoshinaga,[a] Josene M. Toldo,[b] Willian R. Rocha *[a] and Mario Barbatti *[bc]

Received 12th June 2024,
Accepted 6th August 2024

DOI: 10.1039/d4cp02373k

rsc.li/pccp

Resveratrol is well-known for promoting health benefits due to its antioxidant, anti-aging, anti-carcinogenic, and other beneficial activities. Understanding the photophysics of resveratrol is essential for determining its applicability to pharmaceutical innovations. In the present work, we used an explore-then-assess strategy to map the internal conversion pathways of *trans*-resveratrol. This strategy consists of exploring the multidimensional configurational space with nonadiabatic dynamics simulations based on a semiempirical multireference method, followed by a feasibility assessment of reduced-dimensionality pathways at a high *ab initio* theoretical level. The exploration step revealed that internal conversion to the ground state may occur near five distinct conical intersections. The assessment step showed that the main photoisomerization pathway involves a twisted-pyramidalized S_1/S_0 conical intersection, yielding either *trans* or *cis* isomers. However, a secondary path was identified, where *cis*-*trans* isomerization happens in the excited state and internal conversion occurs at a cyclic conical intersection, yielding a closed-ring resveratrol derivative. This derivative, which can be formed through this direct path or an indirect photoexcitation, may be connected to the production of oxygen-reactive species previously reported and have implications in photodynamic therapy.

1. Introduction

Resveratrol (3,4′,5-trihydroxy-stilbene) is a natural polyphenol present in various plants and fruits, particularly in grape skins.[1] The interest in this molecule began with the "French Paradox," the improved cardiovascular condition in French people despite a high saturated fat diet, a phenomenon associated with moderate wine consumption.[2,3] Since then, resveratrol has garnered significant attention for its wide range of pharmacological activities, including antioxidant, anti-aging, anti-inflammatory, anti-diabetic, and anti-cancer properties.[4–6] Its antioxidant activity is related to the ability of peroxyl radicals, formed in the lipid peroxidation chain, to extract H atoms from resveratrol's hydroxyl groups, forming stable radical species.[7,8] This free radical scavenging process can stop the chain reactions involved in oxidative stress.

Resveratrol is found in nature in two isomeric forms, *trans* (Fig. 1a) and *cis* (Fig. 1b). The *trans* isomer is the most stable and abundant and is associated with its numerous health benefits.[9] The *cis*-isomer is unstable, but it can be found in smaller proportions in food products.[7] This isomer can be obtained by exposing the *trans*-isomer to UV radiation or high

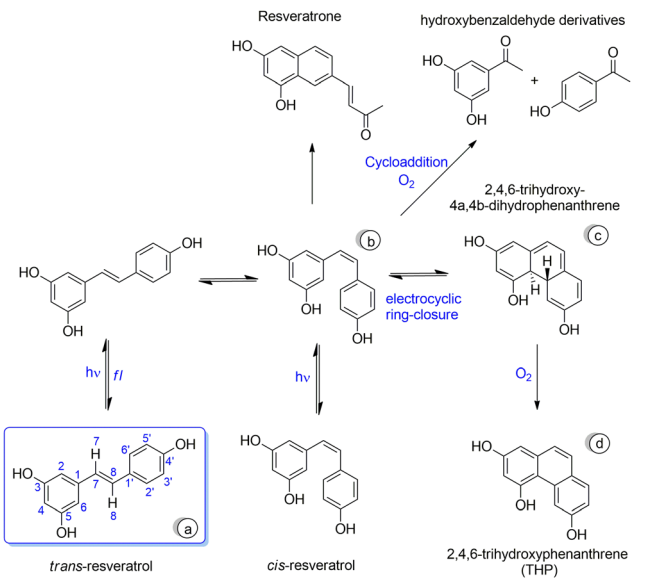

Fig. 1 Structures of (a) *trans*-resveratrol, (b) *cis*-resveratrol, (c) 2,4,6-trihydroxy-4a,4b-dihydrophenanthrene and (d) 2,4,6-trihydroxy-phenanthrene.

[a] *Laboratório de Estudos Computacionais em Sistemas Moleculares, eCsMo, Departamento de Química, ICEx, Universidade Federal de Minas Gerais, Belo Horizonte, Minas Gerais, Brazil. E-mail: wrocha@ufmg.br*
[b] *Aix Marseille University, CNRS, ICR, Marseille, France. E-mail: mario.barbatti@univ-amu.fr*
[c] *Institut Universitaire de France, 75231 Paris, France*

† Electronic supplementary information (ESI) available: Computational details, distribution of hopping geometries, orbital characterization, and Cartesian coordinates of all stationary structures and conical intersections are given in the ESI. See DOI: https://doi.org/10.1039/d4cp02373k

pH conditions,[10] and the isomerization yield is highly dependent on the experimental conditions, such as time, concentration, and light source.[11,12] When an ethanol solution of *trans*-isomer is irradiated with a 365 nm light source or under solar radiation, its photodegradation profile fits a first-order kinetic model with a half-life $t_{1/2}$ = 2.8 and 10.5 min.[11] Under the same conditions, the *cis*-isomer half-life was determined as $t_{1/2}$ = 10.8 and 50.6 min. When *trans*-resveratrol was irradiated at 254 nm—that is, above its absorption maxima in ethanol, 305 nm[12]—the conversion to the *cis*-isomer was much faster and could not be determined.[11] Dzeba *et al.* determined a unimolecular excited state decay rate constant k_d = 1/(28.6 ps) for *trans*-resveratrol excited at 355 nm in acetonitrile.[13] The low fluorescence quantum yield (Φ_f = 0.03) indicates that this molecule is mostly deactivated *via* nonradiative internal conversion to the ground state by either returning to the original isomer or forming the photoisomer (Φ_{iso} = 0.20). In their experiments, Dzeba *et al.* discarded the triplet formation, as the S_1 state decays entirely within tens of picoseconds.[13]

The mechanisms of this *trans*/*cis* photoisomerization are not yet fully understood. Experimental studies point out competitive pathways after *trans*-resveratrol photoexcitation, revealing not only the formation of *trans*- and *cis*-resveratrol but also other byproducts. One of these compounds is the potentially harmful 2,4,6-trihydroxyphenanthrene (Fig. 1d), which originates from the *cis*-isomer through a 6π-electrochemical photocyclization (Fig. 1c) and subsequent oxidation.[7,12,14] Other products derived from the fragmentation of the *cis*-isomer are also reported, such as those shown in Fig. 1.[7,15] Under different experimental conditions, a fluorescent compound known as resveratrone was also identified.[11,16] Several works reported that resveratrol after excitation, acts as a photosensitizer producing singlet oxygen, holding great potential for applications in photodynamic therapy.[12,17,18] This reactive oxygen species can then be used to eliminate microorganisms. Dos Santos and colleagues demonstrated that upon photoexcitation, *trans*-resveratrol produced singlet oxygen, leading to the inactivation of *Staphylococcus aureus* pathogens.[19] Although the researchers were unable to identify which derivative of resveratrol was responsible for the production of the reactive oxygen species, the results provided evidence for the potential use of photoactivated *trans*-resveratrol in antimicrobial photodynamic therapy.

Resveratrol is a derivative of stilbene, and its photochemical reactivity is likely related.[7,12] Therefore, it is relevant to survey what is known about stilbene photoisomerization. Extensive discussions about the photoisomerization of stilbene mainly concern the existence of a *phantom state*, a critical reactive intermediate in the S_1 surface of both *cis*- and *trans*-stilbene.[20–26] This elusive state, commonly referred to as a perpendicular state (1p*), has a twisted geometry around the ethylenic C=C bond. It is dark and short-lived, making it challenging to observe experimentally. This state relaxes to the ground state *via* a closely located conical intersection.[20,27,28] The much slower isomerization of the *trans*-isomer (~100 fs) compared to the *cis*-isomer (~1 ps) is attributed to a barrier (~3 kcal mol^{-1}) from the S_1 minimum to the 1p* state in the *trans*-stilbene. In contrast, in the *cis*-isomer, this conversion is nearly barrierless.[21,24,29–31] This considerably large lifetime difference has significant implications for the photoisomerization mechanism of the two isomers.[32]

Competitive pathways are also observed in the isomerization of stilbenes. As in resveratrol, phenanthrene is formed from an unstable, short-lived, and readily oxidable dihydrophenanthrene (DHP).[33] It has been found that phenanthrene formation primarily occurs from the excitation of *cis*-stilbene,[33] although early works postulate that DHP can also be formed after the excitation of a *trans*-isomer through a *cis*-excited intermediate.[34–36] However, the cyclization is expected to be a minor channel in the photophysics pathway, with solutions of excited *cis*-stilbene giving rise to phenanthrene with a quantum yield smaller than 0.19.[34]

Much less detail is known about the photoisomerization of *trans*-resveratrol. Since its biological activity is affected by its stereoisomerism, a fundamental understanding of the photostability of *trans*-resveratrol is essential to assess its own application and its photoproducts as potential therapeutical agents. Yet, the photochemistry of resveratrol is computationally underexplored,[7,35] and no dynamical investigation exists. With this goal in mind, we aimed to employ computational chemistry methods to explore the *trans*-resveratrol photoisomerization pathways in the gas phase, filling this knowledge gap and establishing high-level theoretical reference data for further computational and experimental resveratrol investigations.

Exploring photoisomerization is challenging when dealing with large molecules with significant conformation flexibility, like resveratrol, due to the multiple reaction pathways the system can follow. The anharmonicity and diabatic diversity of the excited-state potential energy surfaces almost always reveal pathways far from those our chemical intuition expects, or trivial reaction coordinates suggest.[36–38] Here, we introduce the explore-then-assess strategy, which we developed to face this challenge. This strategy starts with a low accuracy yet computationally fast semiempirical multireference method to perform nonadiabatic dynamics simulations. Such simulations populate the configurational space, revealing multiple potential internal conversion pathways beyond trivial guesses such as single-torsional isomerization. Then, we assess the feasibility of these numerous pathways through potential energy profile calculations with a high-level accurate method extended multi-state complete active space second-order perturbation (XMS-CASPT2). The explore-then-assess strategy successfully allowed us to determine the possible fates of photoexcited resveratrol, as we discuss in the Results and discussion section.

2. Computational details

Nonadiabatic dynamics simulations in the gas phase were performed using surface hopping in combination with the multireference configuration interaction based on orthogonalization- and dispersion-corrected semiempirical method 2 (ODM2/MRCI) available in the MNDO program.[39] To enable these simulations, we implemented a new interface between

MNDO[40] and Newton-X CS.[41] In the MRCI treatment,[42] the active space consisted of 24 electrons in 18 orbitals, generating configurations from three reference configurations.

The initial conditions for the dynamics were sampled from a harmonic oscillator Wigner distribution of the nuclei at a temperature of 0 K. 1000 random structures were generated and used to compose the absorption spectrum with the nuclear ensemble approach (NEA).[43] The initial conditions were restricted to two excitation windows, the first at 3.9 ± 0.1 eV and the second at 4.5 ± 0.1 eV, corresponding to the initial region and the peak of the compound's absorption band calculated with the semiempirical method.

For each excitation window, we ran 100 trajectories of 1000 fs using the decoherence-corrected fewest switch surface hopping approach (DC-FSSH).[44] The classical equations were integrated with the Velocity Verlet algorithm with a time step of 0.1 fs.[45] The quantum equations were integrated with a 0.005 fs time step, using interpolated quantities between classical steps. Dynamics started in the S_1 state, and all electronic states up to S_2 were included in the dynamics. In the case of frustrated hoppings, the momentum direction was unchanged. Decoherence was corrected with the simplified decay of mixing with the usual value of 0.1 a.u. for the α parameter.[46] The results were analyzed statistically using the ULaMDyn program.[47]

To overcome issues coming from orbital rotations within the active space during the dynamics, we did not impose the usual total energy conservation constraints but let the dynamics freely evolve. This renders unreliable results for statistical analysis but does not affect the main objective of these simulations, which was to explore possible pathways for the deactivation of *trans*-resveratrol after photoexcitation. In our simulations, we used ODM3/MRCI for spectrum and initial conditions and ODM2/MRCI for dynamics. These two ODM*x* versions deliver broadly similar results for resveratrol, and this minor inconsistency can be entirely overlooked, especially given the exploratory character of the dynamics. This methodology was chosen for its efficiency in describing the characteristics of excited states.[48,49] ODM2/MRCI also demonstrates a good capability for describing conical intersections while maintaining an attractive computational cost.

Once we had the possible internal pathways from dynamics simulations, we computed their potential energy profiles using the extended multi-state complete active space second-order perturbation theory (XMS-CASPT2)[50] with the ANO-RCC-VDZP basis set based on structure optimized with the complete active space self-consistent field (CASSCF) method[51] with the ANO-*S*-VDZP basis set.[52] The active space comprised 10 electrons and 10 orbitals, and the state average (SA) was performed over 5 states. The active space included π, π^* orbitals of the central C=C bond and the aromatic rings (Fig. S1, ESI†).

SA5-CASSCF(10,10)/ANO-S-VDZP was used to optimize the stationary structures of *trans*- and *cis*-resveratrol in the S_0 and S_1 states. The structures of the conical intersections were also optimized at the same level, except for a conical intersection involving hydrogen dissociation. In that case, the σ and σ^* orbitals of the dissociated O–H bond were also included in the active space. The energy threshold for the convergence criteria of the conical intersections was 10^{-4} a.u. Subsequently, the energies of all optimized structures were corrected using XMS-CASPT2/ANO-RCC-VDZP with the same (10,10) active space. These calculations were performed with IPEA shift[53] set to zero and an imaginary level shift of 0.1 a.u.,[54] which represents a good compromise between preventing the occurrence of intruder states while still maintaining a good amount of dynamic correlation. As the IPEA shift dilemma is not entirely settled,[55,56] we also tested an IPEA shift of 0.25. Potential energy profiles using linear interpolation in internal coordinates (LIIC) calculations between the S_1 minima and the conical intersections were performed using XMS-CASPT2. All multiconfigurational calculations were performed using the OpenMolcas 19.11 program.[57]

3. Results and discussion

3.1. Absorption spectrum of *trans*-resveratrol

The ground state structure of *trans*-resveratrol was optimized at the multireference configuration interaction based on ODM3/MRCI from Dral, Wu, and Thiel.[39] No imaginary frequencies were observed in the normal-mode analysis. The ground state was also optimized at CASSCF level. The excited state energies were computed using XMS-CASPT2. The active orbitals selected for the CASSCF(10,10) calculations are shown in Fig. S1 (ESI†), after a benchmark to determine the choice of the active space. The results were highly consistent between the two methods. Calculating the root mean square deviation (RMSD) value between the two optimized structures resulted in a value of 0.07 Å displacement (Fig. S3, ESI†). The vertical spectrum computed with both methods is characterized in Table 1. The transition moments were obtained from dipole length formulation using the XMS-CASPT2 transition density and the molecular orbitals representing the electronic transitions are given in the ESI† Fig. S4. Also, a comparison between vertical excitation energies using different IPEA shift values and basis sets is shown in the ESI† Table S2.

Both results showed the S_1 state as a bright state. The excitation energy values obtained using the two methods were similar, with a difference of only 0.17 eV for the excitation energy of the bright state. Additionally, the character and order of the orbitals involved in the transitions from the S_0 to the excited S_1, S_2, and S_3 state obtained with XMS-CASPT2 and ODM3/MRCI were the same (Fig. S4, ESI†).

Next, we computed the absorption spectrum of *trans*-resveratrol in the gas phase using the nuclear ensemble

Table 1 Vertical excitation energies and oscillator strength (*f*) for *trans*-resveratrol at the ODM3/MRCI and XMS-CASPT2 levels. The main orbital transitions are indicated in the ESI Fig. S4

	XMS-CASPT2//CASSCF		ODM3//ODM3	
S_0 Geom	Energy (eV)	*f*	Energy (eV)	*f*
S_1	4.10	0.986	4.63	1.093
S_2	4.73	0.009	5.02	0.026
S_3	4.90	0.008	5.17	0.048

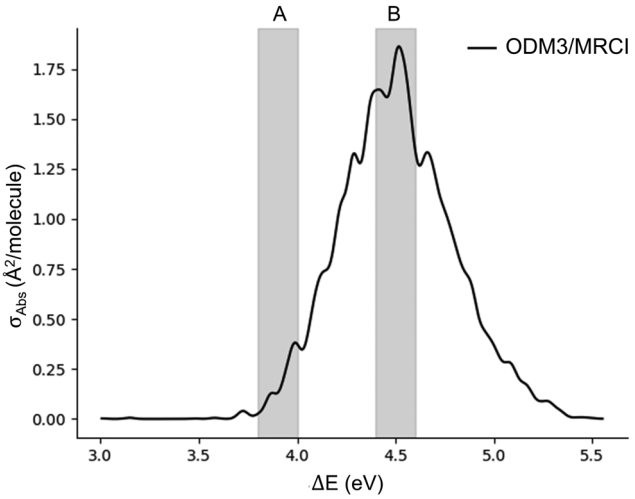

Fig. 2 The absorption spectrum of *trans*-resveratrol at the ODM3/MRCI level. The shaded regions indicated the excitation windows employed in the exploratory dynamics.

method[58] (Fig. 2). This spectrum features a bright absorption band centered at 4.5 eV, primarily corresponding to the S_1 $\pi\pi^*$ transition seen in Table 1. We also aimed to determine whether *trans*-resveratrol excitation at different regions of the compound's absorption spectrum would result in different reaction pathways. Thus, we selected geometries and velocities to start our dynamics simulations from two different spectral windows: one at the band origin (shaded region A at 3.9 ± 0.1 eV) and the other at the band maximum (shaded region B at 4.5 ± 0.1 eV).

3.2. Explore-then-assess strategy

3.2.1. Exploration step: semiempirical nonadiabatic dynamics. Nonadiabatic dynamics simulations of photoexcited *trans*-resveratrol in the gas phase were performed using surface hopping[44,46] based on ODM2/MRCI.[39] The goal of these simulations is to explore the configurational space to reveal the possible isomerization mechanisms. The idea of exploring the configurational space to identify different photochemical pathways was introduced by Pieri *et al.*[59] in the so-called nanoreactor.

Using ODM*x*/MRCI for exploratory dynamics brings several benefits. It is computationally inexpensive, with much lower costs than the main alternative, linear-response time-dependent density functional theory (TDDFT).[60] Thus, ODM/MRCI allows simulations of large molecular systems, longer trajectories, multiple excited states, and reduced time steps (which is a crucial feature to avoid troubles with the so-called trivial (or not avoided) crossings[61]). Second, ODM*x*/MRCI naturally includes double and higher excitations, a feature missing in TDDFT[62] and other low-cost methods such as algebraic diagrammatic construction to second-order (ADC(2)).[63] Finally, the multireference character of ODM*x*/MRCI implies a correct description of the branching space surrounding conical intersections. Again, methods like TDDFT and ADC(2) fail in this task, delivering wrong dimensionality branching spaces with potentially deleterious consequences for the dynamics.[64]

During the nonadiabatic dynamics simulations, *trans*-resveratrol repopulated the ground state by hopping from the first excited state. The $S_1 \rightarrow S_0$ hopping geometries, a proxy for the nearest conical intersection driving the internal conversion, were classified. Visual inspection of these structures revealed that dihedral angles C1–C7–C8–C1′ and H7–C7–C8–H8 were the critical coordinates determining the main types of S_1/S_0 intersections. The distribution of the hopping structures characterized by these two dihedral angles is shown in Fig. 3. In this figure, it is possible to observe five main clusters of hopping geometries. We refer to these points as crossing regions (in the following section, we will show that each of these regions is associated with a distinct conical intersection). The number of

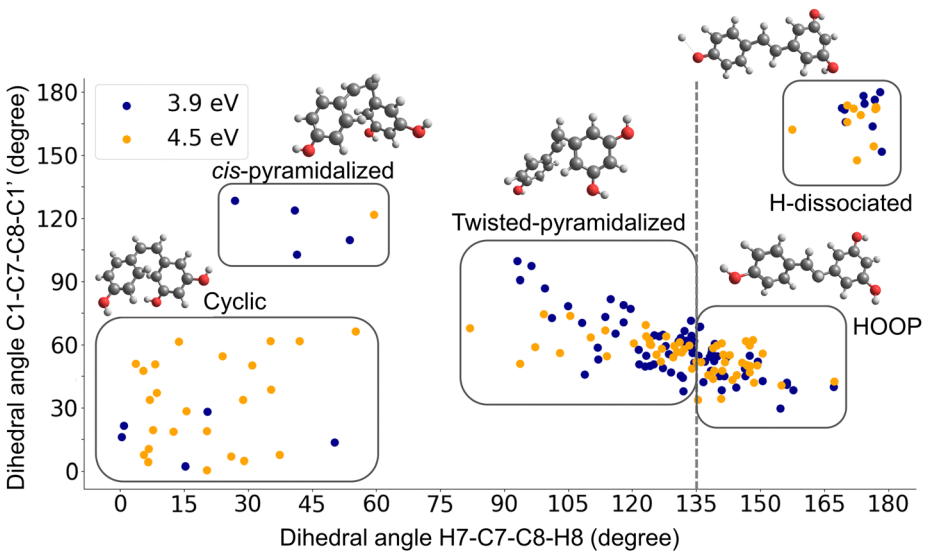

Fig. 3 Hopping structures obtained after excitation at the origin (3.9 eV) of the absorption band (blue dots) and at the maximum (4.5 eV) of the absorption band (orange dots). These structures can be separated into five clusters corresponding to different regions of the S_1/S_0 crossing seam.

hopping structures in each of these clusters is given in the ESI† Table S1. The five types of S_1/S_0 hopping geometries include (i) a *cis*-resveratrol with pyramidalization of C7 (*cis*-pyramidalized); (ii) a structure with H extraction from the hydroxyl at the *para* position of *trans*-resveratrol (H-dissociated); (iii) a twisted-pyramidalized structure; (iv) a structure where one can observe a tendency of ring closure through the C6′–C2 bond of *cis*-resveratrol (cyclic); (v) a structure with H7 and H8 out of the plane plus pyramidalization of C7 (HOOP).

Although in Fig. 3, the ensemble of points classified as twisted-pyramidalized and HOOP seems to form a single cluster, an inspection of the structures shows that they belong to different categories depending on whether their H7–C7–C8–H8 dihedral angle is bigger or smaller than 135°. This occurs due to the relative orientation of the phenol rings, which is not captured by the two dihedral angles plotted in the figure.

The same five types of hopping structures appeared in both excitation windows. Nevertheless, given the exploratory character of these results, we prefer not to discuss the quantitative distributions shown in Fig. 3.

3.2.2. Assessment step: high-level potential energy profiles. The dynamics based on ODM2/MRCI should be taken as a qualitative approach to explore the configurational space due to the inaccuracies intrinsic to any parameterized method and also the frequent potential energy surface discontinuities caused by orbital rotations into the active space. Therefore, the hopping distribution of the geometries shown in Fig. 3 does not reliably predict the distribution of internal conversion pathways. Nonetheless, this does not affect the main objective of these simulations, which was solely to explore possible pathways for the deactivation of photoexcited *trans*-resveratrol. Therefore, the next step was to investigate the potential energy pathways to each of the crossing regions with a high-level quantum chemical method. To this end, we adopted the well-established protocol of computing CASPT2 energies on CASSCF-optimized structures.[65]

We started by optimizing *trans*- and *cis*-resveratrol S_0 and S_1 minima with CASSCF. We also optimized the closed ring S_0 structure (Fig. 1c). All attempts to optimize an S_1 minimum of this structure resulted in an S_1/S_0 conical intersection. We also used CASSCF to search and optimize the S_1/S_0 conical intersections corresponding to each of the five crossing structures discussed in the previous section. The XMS-CASPT2 energies of all minima and conical intersections are reported in Table 2. Their geometries are shown in Fig. 4 and their Cartesian coordinates are given in the ESI.† The twisted-pyramidalized structure was anticipated as a possible conical intersection, based on previous studies of stilbene, which reported the existence of the phantom structure with perpendicular aromatic rings.[20,27] Furthermore, there are descriptions in the literature of the cyclized structure being observed after the excitation of *cis*-stilbene,[20,66] which suggests that this structure might also be a conical intersection in resveratrol. Structures such as *cis*-pyramidalized and HOOP were revealed by our exploratory simulation as well as the possibility of crossing regions that were not chemically intuitive, such as hydrogen dissociation.

Table 2 XMS-CASPT2 energies of the minima and conical intersections (CoIn) of resveratrol optimized with CASSCF. Energies relative to the *trans*-resveratrol ground state. Oscillator strengths are given in parentheses. For the conical intersections, S_1 and S_0 energies are not degenerated because of this difference in the computational levels. Thus, the energy values presented for the conical intersections refer to the averages of the energy values of the S0 and S1 states

	Relative energies (eV)	
Structure	S_0	S_1
Trans S_0 minimum	0.00	4.10
Trans S_1 minimum	0.87	4.03 (0.986)
Cis S_0 minimum	0.09	4.50
Cis S_1 minimum	1.39	4.01 (0.456)
Closed ring S_0 minimum	1.44	3.97
H dissociated CoIn	5.70	
Cis-pyramidalized CoIn	6.16	
Twisted-pyramidalized CoIn	3.73	
HOOP CoIn	5.14	
Cyclic CoIn	2.84	

To investigate the reaction coordinates between the S_1 minima and the different conical intersections, we created linearly interpolated internal coordinates (LIIC) reaction pathways between these structures. Finally, we computed XMS-CASPT2 energies for all points along these paths (Fig. 5). This protocol yields reliable potential energy profiles but has two well-known drawbacks. First, because the intermediary points along the pathways are not optimized, the reaction barriers are necessarily overestimated unless the reaction is fast enough to happen with all other coordinates resting frozen. Second, because the XMS-CASPT2 calculation is done on a CASSCF geometry, the calculation of the conical intersection structure renders a relatively large energy gap between the crossing states. The following analysis considers these issues.

All energy profiles are plotted in Fig. 5, as a function of mass-weighted generalized coordinates. These coordinates at point i of the profile are computed as $\rho_i = [\Sigma_\alpha M_\alpha (R_{ia} - R_{0\alpha})^2]^{1/2}$ where the sum is over all atoms a with mass M_α, $R_{i\alpha}$ is the Cartesian coordinate of the atom a at point i, and R_{0i} is the Cartesian coordinates of the first point in the profile. Describing the energy profiles in terms of mass-weighted coordinates directly delivers information on how much distortion is needed for the molecule to move on that reaction pathway. A path with a significant energy barrier but a short mass-weighted distance may predominate over another with a low energy barrier but requiring more extensive mass-weighted distortions. To discuss the potential energy profiles, we always assume that *trans*-resveratrol vibrationally relaxes to the *trans*-S_1 minimum before moving toward the crossing region. Thus, unless otherwise indicated, the *trans*-S_1 minimum is the starting point in the energy profile.

The energetically most favorable energy profile is the path from the *trans*-S_1 to the twisted-pyramidalized structure (Fig. 5b), which does not exhibit a barrier. However, it requires large mass rearrangements of the order of 22 $amu^{1/2}$ Å, which may reduce its effectiveness or elongate the internal conversion lifetime. This crossing region can spawn both *trans*- and *cis*-resveratrol in the ground state. Comparing the obtained result with previous

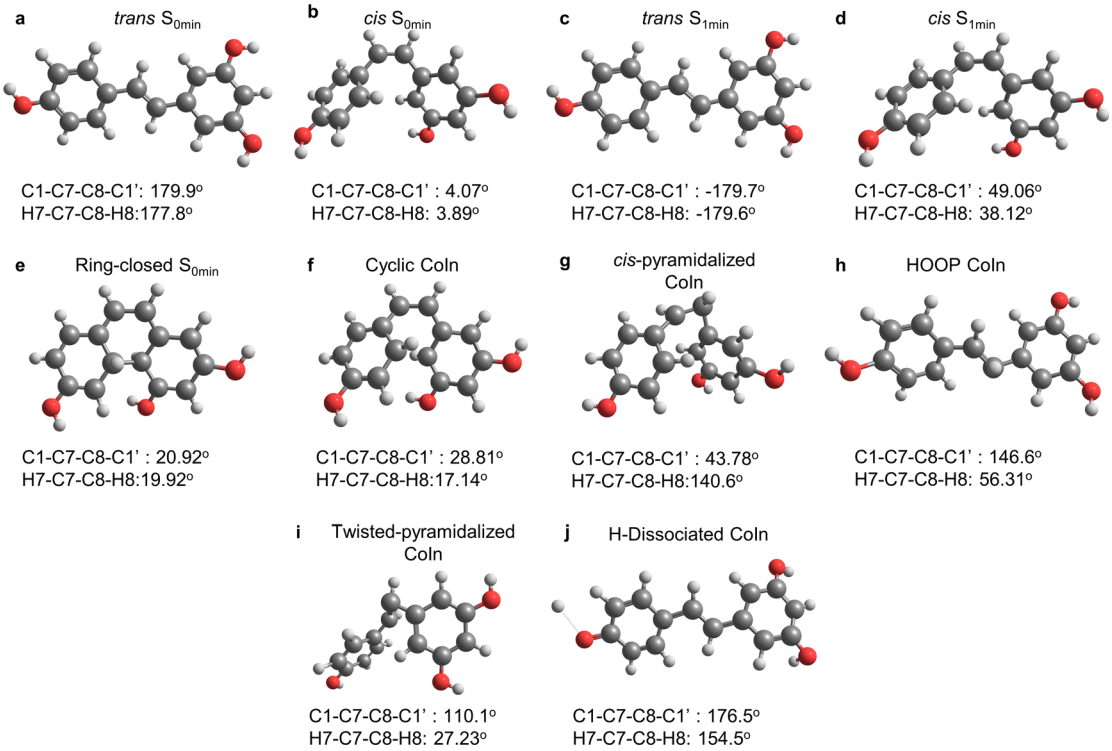

Fig. 4 CASSCF(10,10) optimized geometries of minima and S_1/S_0 conical intersections (CoIn) used in the linear interpolation of the potential energy profiles.

literature studies conducted with stilbene,[20] a similarity between the photoisomerization processes of resveratrol and stilbene is that both pass through intermediates that exhibit twisting between the aromatic rings[20,21,67] and pyramidalization of one of the carbon atoms of the central double bond,[27,68] but unlike stilbene, which undergoes *trans-cis* isomerization with a barrier of 3 kcal mol^{-1},[20] the photoisomerization of *trans*-resveratrol occurs without barrier.

The potential energy profile between the *trans*-S_1 minimum and the S_1/S_0 HOOP conical intersection (Fig. 5a) reveals the existence of a maximum energy barrier of 1.11 eV (25.60 kcal mol^{-1}) for the conversion to occur. The observed mass-weighted distortion was close to 7 $amu^{1/2}$ Å, indicating that the conversion would occur without significant structural changes in the molecule. However, the identified barrier suggests that such conversion is unfavorable after *trans*-resveratrol excitation to its first excited singlet state. Excitations to higher-energy singlet states would be necessary for reaching the HOOP conical intersection. The same conclusion can be drawn concerning the H-dissociated pathway (Fig. 5c), which presents a maximum barrier of 1.67 eV (38.5 kcal mol^{-1}). This high barrier indicates that the conversion is unlikely to occur through this path.

We also computed the barriers for the *trans*-to-*cis* isomerization in the S_1 state. As seen in the potential energy profile between *trans*-S_1 and *cis*-S_1 minima (Fig. 5d), this reaction pathway has a maximum barrier of 1.32 eV (30.4 kcal mol^{-1}) and a mass-weighted distortion close to 27 $amu^{1/2}$ Å. This indicates that a significant structural distortion and a prohibitive amount of energy are required for the isomerization to occur.

Nevertheless, we found out that *trans-to-cis* photoisomerization in the excited state can, in principle, occur during relaxation toward the twisted-pyramidalized conical intersection. When crossing this nonadiabatic region, resveratrol may remain on the S_1, moving toward the *cis* isomer. This path is illustrated in the potential energy profile between the twisted-pyramidalized conical intersection and the *cis*-S_1 minimum in Fig. 5e. A relatively small maximum barrier of 0.64 eV (14.7 kcal mol^{-1}) was observed, implying that the reaction pathway is feasible.

We now assume that the *cis*-S_1 isomer is populated. This population can arrive either from excited-state isomerization (as discussed in Fig. 5e) or *via* a subsequent photoexcitation of the *cis*-isomer in the ground state after internal conversion at the twisted-pyramidalized conical intersection (Fig. 5b). In the case of this second excitation, note that the vertical excitation energy of the *cis*-structure (4.41 eV at XMS-CASPT2) is larger than that of the *trans* (4.10 eV). This variation between the wavelengths of maximum absorption of the *cis* and *trans* isomers was expected. Experimental results show that in aqueous solution, the maximum absorption of *cis*-resveratrol occurs at 286 nm, while that of *trans*-resveratrol occurs at 304 nm.[69] Despite that, the energy of 4.10 eV allows the excitation of *cis*-resveratrol in regions outside the maximum absorption due to the compound's absorption bandwidth.

Either way, once the *cis*-S_1 minimum is populated, the pathway toward the cyclic conical intersection (Fig. 5g) is highly favorable. It presents no barrier and requires a modest distortion of about 13 $amu^{1/2}$ Å. Internal conversion at this conical intersection should deliver large yields of the closed-ring structure of

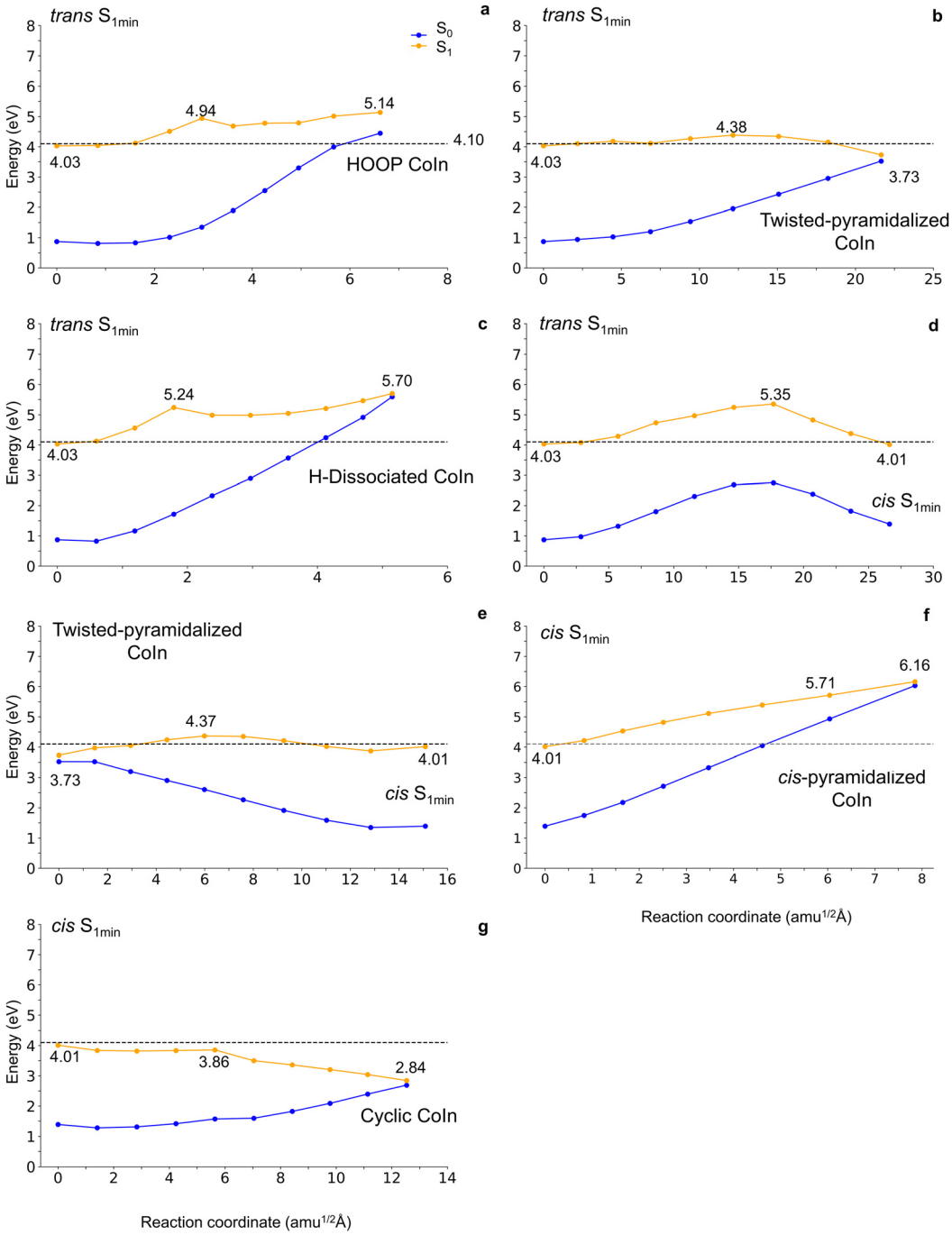

Fig. 5 Energy profiles between the *trans*-S_1 minimum and the (a) HOOP conical intersection, (b) twisted-pyramidalized conical intersection, (c) H-dissociated conical intersection, (d) *cis*-S_1 minimum. Energy profiles between (e) twisted-pyramidalized conical intersection and *cis*-S_1 minimum, (f) *cis*-S_1 minimum and *cis*-pyramidalized conical intersection, (g) *cis*-S_1 minimum and cyclic conical intersection. All energy profiles were done with XMS-CASPT2 on CASSCF energies, which explains the non-null energy gaps at the conical intersections.

resveratrol. The formation of a cyclized conical intersection was also observed in the internal conversion of *cis*-stilbene before reaching the closed-ring structure.[27] The *cis*-S_1 population can alternatively convert to the ground state at the twisted-pyramidalized conical intersection (Fig. 5e starting from the right to left). The potential energy profile between the *cis*-S_1 minimum and *cis*-pyramidalized conical intersection (Fig. 5f) shows a prohibitive barrier of 2.15 eV (49.6 kcal mol^{-1}) and should not be accessed.

As resveratrol is a stilbene derivative, we can draw some parallels between the dynamics of these two molecules. The first observation is that the most accessible conical intersections found for resveratrol were also found for stilbene. In the study conducted by Weir *et al.* using *ab initio* multiple

spawning together with CASSCF(2,2),[27] they reported an orthogonal branching on the S_1 state of isolated *cis*-resveratrol. One of these branches is cyclization, which originates DHP and *cis*-isomer through a DHP-like cyclic conical intersection. This is analogous to our findings for resveratrol passing through the cyclic CoIn. The second (and dominant) branch is the isomerization coordinate, which gives rise to *trans*- and *cis*-stilbene. In this case, two avoided crossing regions were observed. One of them (they call the CoIn associated with it Pyr-Mig(Ph)-CI) displays pyramidalization and rotation of the phenyl group; it is analogous to our twisted-pyramidalized CoIn (see comparisons in the ESI,† Fig. S6). The second one, whose intersection the name Pyr-Mig(H)-CI, also displays pyramidalization but with a more substantial degree of hydrogen displacement and a smaller twisting dihedral angle; this structure is similar to what we refer to as HOOP CoIn here.

For stilbene, the splitting between the two competing isomerization CoIns is approximately half-half.[27] However, for resveratrol, our calculations indicate that following the twisted-pyramidalized CoIn is preferential, as the PES towards the HOOP CoIn involves an energy barrier of 1.1 eV. We are tempted to attribute this effect to the presence of the hydroxyl groups in resveratrol. However, a direct comparison is not possible given the different levels of theory used in the two works, and it is out of the scope of the present manuscript. Another important factor contributing to those differences is that our study starts from the *trans*-isomer, while Weir and collaborators initiated their dynamics from *cis*-resveratrol.

Furthermore, our semiempirical dynamics also revealed other alternative deactivation routes passing through a *cis*-pyramidalized CoIn or H-dissociated CoIn. These alternative routes are not reported for stilbene (the last one for obvious reasons). We may blame the presence of -OH groups for that. Nevertheless, our PES calculations revealed a significant barrier to reaching those conical intersections, thereby discarding their contribution to the deactivation of resveratrol.

We also considered the involvement of triplet states, despite the experimental evidence from Dzeba *et al.*[13] discarding intersystem crossing (ISC) within tens of ps. We estimated the ISC rate using a path integral approach relying on the harmonic oscillator approximation[70] as implemented in ORCA. Our results show that ISC involving the S_1 states of *trans* and *cis*-resveratrol to the triplet manifold occurs at time scales of seconds and microseconds, respectively (ESI,† Table S3). These numbers indicate that these processes are non-competitive with internal conversion, aligning with the experimental results from Dzeba *et al.*[13]

4. Conclusions

This work delivers high-level reference data for *trans*-resveratrol photoisomerization pathways in the gas phase. These data result from a novel computational strategy named explore-then-assess. It consists of exploring the multidimensional configurational space with fast semiempirical nonadiabatic dynamics to reveal the potential reaction pathways and assessing their importance through static high-level multiconfigurational calculations. The leading isomerization pathways are schematically summarized in Fig. 6.

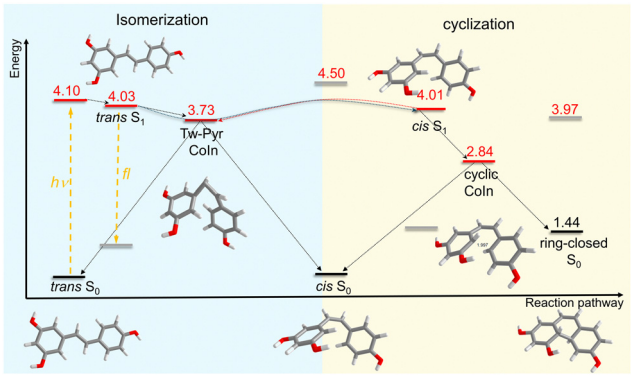

Fig. 6 Schematics of the most likely photoisomerization pathways of *trans*-resveratrol.

The exploration step, based on semiempirical ODM2/MRCI, revealed five S_1/S_0 crossing regions, denoted as *cis*-pyramidalized, cyclic, twisted-pyramidalized, HOOP, and H-dissociated. The assessment through linear interpolation in internal coordinates computed with XMS-CASPT2 showed that internal conversion should primarily occur at the twisted-pyramidalized conical intersection, which has no energy barrier starting from the *trans*-S_1 minimum. The reaction pathways from the *trans*-S_1 state to HOOP and H-dissociated conical intersections were prohibitive due to high energy barriers. However, they may be activated if the initial excitation were to a higher-energy singlet excited state.

After reaching the twisted-pyramidalized crossing region, resveratrol should mainly relax to the ground state, yielding *trans* and *cis* ground state isomers. Additionally, resveratrol can also pass through this region, remaining in the excited state and forming the *cis*-S_1 structure. This pathway opens the possibility of *trans-cis* photoisomerization even in the excited state.

Alternatively, *cis*-S_1 can also be formed *via* a subsequent excitation of ground-state *cis*-isomer resulting from the initial isomerization process. Once the *cis*-S_1 isomer is populated, it can return to the ground state *via* an energetically and geometrically favorable cyclic conical intersection, which should have a closed-ring resveratrol derivative as a leading product.

This work has allowed us to understand the photophysics of *trans*-resveratrol internal conversion in the gas phase, including the pathways for photoisomerization and the generation of cyclized products. The study establishes a high-level dataset, serving as a reference for subsequent fundamental and applied research on resveratrol and its derivatives, even under other solvent conditions. Along this line, we are currently studying processes involving intersystem crossing from cyclic derivatives of resveratrol to triplet states and investigating the involvement of resveratrol in singlet oxygen generation, paving the way for its potential in photodynamic therapy.

Author contributions

Supervision: JMT, MB; project administration: MB; funding acquisition: WR, MB; methodology: JMT, MB; analysis: MY; investigation: MY; visualization: MY; writing – original draft: MY; writing – review & editing: MY, JMT, WR, MB.

Data availability

The data supporting this article have been included as part of the ESI.†

Conflicts of interest

The authors declare no conflict of interest.

Acknowledgements

MY and WR thank CNPq (Conselho Nacional de Desenvolvimento Científico e Tecnológico, INCT-Catálise) and FAPEMIG (Fundação de Amparo à Pesquisa do Estado de Minas Gerais) for financial support and research grants. They also thank the Institutional Internationalization Program, CAPES PrInt (PRPG 04/2022), for providing funding for MY's doctoral internship at Aix Marseille University. JMT and MB thank the European Research Council (ERC) Advanced grant SubNano (grant agreement 832237). The authors acknowledge the Centre de Calcul Intensif d'Aix-Marseille for granting access to its high-performance computing resources.

References

1 B. Salehi, A. P. Mishra, M. Nigam, B. Sener, M. Kilic, M. Sharifi-Rad, P. V. T. Fokou, N. Martins and J. Sharifi-Rad, *Biomedicines*, 2018, **6**, 91.
2 B. Catalgol, S. Batirel, Y. Taga and N. K. Ozer, *Front. Pharmacol.*, 2012, **3**, 141.
3 M. H. Keylor, B. S. Matsuura and C. R. J. Stephenson, *Chem. Rev.*, 2015, **115**, 8976–9027.
4 L. X. Zhang, C. X. Li, M. U. Kakar, M. S. Khan, P. F. Wu, R. M. Amir, D. F. Dai, M. Naveed, Q. Y. Li, M. Saeed, J. Q. Shen, S. A. Rajput and J. H. Li, *Biomed. Pharmacother.*, 2021, **143**, 112164.
5 B. Ren, M. X. Y. Kwah, C. Liu, Z. Ma, M. K. Shanmugam, L. Ding, X. Xiang, P. C. L. Ho, L. Wang, P. S. Ong and B. C. Goh, *Cancer Lett.*, 2021, **515**, 63–72.
6 T. Meng, D. Xiao, A. Muhammed, J. Deng, L. Chen and J. He, *Molecules*, 2021, **26**, 229.
7 R. Á. Rodríguez, I. R. Lahoz, O. N. Faza, M. M. Cid and C. S. Lopez, *Org. Biomol. Chem.*, 2012, **10**, 9175–9182.
8 R. Amorati and L. Valgimigli, *Org. Biomol. Chem.*, 2012, **10**, 4147–4158.
9 C. Leischner, M. Burkard, A. Michel, S. Berchtold, H. Niessner, L. Marongiu, C. Busch, J. Frank, U. M. Lauer and S. Venturelli, *Molecules*, 2021, **26**, 5586.
10 Š. Zupančič, Z. Lavrič and J. Kristl, *Eur. J. Pharm. Biopharm.*, 2015, **93**, 196–204.
11 T. Rodríguez-Cabo, I. Rodríguez, M. Ramil and R. Cela, *J. Chromatogr. A*, 2015, **1410**, 129–139.
12 Y. Zhao, M. Shi, J. H. Ye, X. Q. Zheng, J. L. Lu and Y. R. Liang, *Food Chem.*, 2015, **171**, 137–143.
13 I. Džeba, T. Pedzinski and B. Mihaljević, *J. Photochem. Photobiol., A*, 2015, **299**, 118–124.
14 A. Francioso, L. Mosca, I. M. Menéndez-Perdomo, S. Fanelli, M. Fontana, M. D'Erme, F. Fuentes-Leon and A. Sanchez-Lamar, *Phytochem. Lett.*, 2019, **30**, 362–366.
15 R. Mattioli, D. Di Risola, R. Federico, A. Ciogli, F. Gasparrini, C. Villani, M. Fontana, A. Maggiore, M. D'erme, L. Mosca and A. Francioso, *Molecules*, 2022, **27**, 2348.
16 I. Yang, E. Kim, J. Kang, H. Han, S. Sul, S. B. Park and S. K. Kim, *Chem. Commun.*, 2012, **48**, 3839–3841.
17 S. Fotiou, D. Fotiou, A. Alamanou and G. Deliconstatinos, *In Vivo*, 2010, **24**, 49–54.
18 I. Lagunes and Á. Trigos, *J. Photochem. Photobiol., B*, 2015, **145**, 30–34.
19 D. P. dos Santos, D. P. Soares Lopes, R. C. de Moraes, C. Vieira Gonçalves, L. Pereira Rosa, F. C. da Silva Rosa and R. A. A. da Silva, *Photodiagn. Photodyn. Ther.*, 2019, **25**, 227–236.
20 N. Minezawa and M. S. Gordon, *J. Phys. Chem. A*, 2011, **115**, 7901–7911.
21 S. A. Kovalenko, A. L. Dobryakov, I. Ioffe and N. P. Ernsting, *Chem. Phys. Lett.*, 2010, **493**, 255–258.
22 P. Tavan and K. Schulten, *Chem. Phys. Lett.*, 1978, **56**, 200–204.
23 G. S. Hammond, J. Saltiel, A. A. Lamola, N. J. Turro, J. S. Bradshaw, D. O. Cowan, R. C. Counsell and V. Vogt, *J. Am. Chem. Soc.*, 1964, **16**, 3197–3217.
24 H. Kuramochi, T. Tsutsumi, K. Saita, Z. Wei, M. Osawa, P. Kumar, L. Liu, S. Takeuchi, T. Taketsugu and T. Tahara, *Nat. Chem.*, 2024, **16**, 22–27.
25 S. Karashima, X. Miao, A. Kanayama, Y. I. Yamamoto, J. Nishitani, N. Kavka, R. Mitric and T. Suzuki, *J. Am. Chem. Soc.*, 2023, **145**, 3283–3288.
26 S. Takeuchi, S. Ruhman, T. Tsuneda, M. Chiba, T. Taketsugu and T. Tahara, *Science*, 2008, **322**, 1073–1077.
27 H. Weir, M. Williams, R. M. Parrish, E. G. Hohenstein and T. J. Martínez, *J. Phys. Chem. B*, 2020, **124**, 5476–5487.
28 M. Williams, R. Forbes, H. Weir, K. Veyrinas, R. J. Macdonell, A. E. Boguslavskiy, M. S. Schuurman, A. Stolow and T. J. Martinez, *J. Phys. Chem. Lett.*, 2021, **12**, 6363–6369.
29 J. S. Baskin, L. Bañ, S. Pedersen and A. H. Zewail, *J. Phys. Chem.*, 1996, **29**, 11920–11930.
30 L. Nikowa, D. Schwarzer, J. Troe and J. Schroeder, *J. Chem. Phys.*, 1992, **97**, 4827–4835.
31 D. C. Todd and G. R. Fleming, *J. Chem. Phys.*, 1993, **98**, 269–279.
32 H. Meier, *Angew. Chem.*, 1992, **31**, 1399–1420.
33 J. Seylar, D. Stasiouk, D. L. Simone, V. Varshney, J. E. Heckler and R. McKenzie, *RSC Adv.*, 2021, **11**, 6504–6508.

34 J.-M. Rodier and A. B. Myers, *J. Am. Chem. Soc.*, 1993, **115**, 10791–10795.
35 J. Del Nero and C. P. De Melo, *Opt. Mater.*, 2002, **21**, 455–460.
36 R. Crespo-Otero, N. Kungwan and M. Barbatti, *Chem. Sci.*, 2015, **6**, 5762–5767.
37 M. Barbatti, *J. Am. Chem. Soc.*, 2014, **136**, 10246–10249.
38 R. Mansour, J. M. Toldo and M. Barbatti, *J. Phys. Chem. Lett.*, 2022, **13**, 6194–6199.
39 P. O. Dral, X. Wu and W. Thiel, *J. Chem. Theory Comput.*, 2019, **15**, 1743–1760.
40 P. O. Dral, X. Wu, L. Spörkel, A. Koslowski, W. Weber, R. Steiger, M. Scholten and W. Thiel, *J. Chem. Theory Comput.*, 2016, **12**, 1082–1096.
41 M. Barbatti, M. Ruckenbauer, F. Plasser, J. Pittner, G. Granucci, M. Persico and H. Lischka, *Wiley Interdiscip. Rev.: Comput. Mol. Sci.*, 2014, **4**, 26–33.
42 A. Koslowski, M. E. Beck and W. Thiel, *J. Comput. Chem.*, 2003, **24**, 714–726.
43 R. Crespo-Otero and M. Barbatti, *Theor. Chem. Acc.*, 2012, **131**, 1–14.
44 J. C. Tully, *J. Chem. Phys.*, 1990, **93**, 1061–1071.
45 W. C. Swope, H. C. Andersen, P. H. Berens and K. R. Wilson, *J. Chem. Phys.*, 1982, **76**, 637–649.
46 G. Granucci and M. Persico, *J. Chem. Phys.*, 2007, **126**, 134114.
47 M. Barbatti, M. Bondanza, R. Crespo-Otero, B. Demoulin, P. O. Dral, G. Granucci, F. Kossoski, H. Lischka, B. Mennucci, S. Mukherjee, M. Pederzoli, M. Persico, M. Pinheiro, J. Pittner, F. Plasser, E. Sangiogo Gil and L. Stojanovic, *J. Chem. Theory Comput.*, 2022, **18**, 6851–6865.
48 J. Jankowska, M. Martyka and M. Michalski, *J. Chem. Phys.*, 2021, **154**, 204305.
49 M. Martyka and J. Jankowska, *J. Photochem. Photobiol., A*, 2023, **438**, 114513.
50 T. Shiozaki, W. Gyroffy, P. Celani and H. J. Werner, *J. Chem. Phys.*, 2011, **135**, 81106.
51 B. O. Roos, P. R. Taylor and P. E. M. Sigbahn, *Chem. Phys.*, 1980, **48**, 157–173.
52 K. Pierloot, B. Dumez, P.-O. Widmark and O. Roos, *Theor. Chim. Acta*, 1995, **77**, 291–306.
53 G. Ghigo, B. O. Roos and P. Å. Malmqvist, *Chem. Phys. Lett.*, 2004, **396**, 142–149.
54 N. Forsberg and A. Malmqvist, *Chem. Phys. Lett.*, 1997, **274**, 196–204.
55 J. P. Zobel, J. J. Nogueira and L. González, *Chem. Sci.*, 2017, **8**, 1482–1499.
56 S. Bai, R. Mansour, L. Stojanović, J. M. Toldo and M. Barbatti, *J. Mol. Model.*, 2020, **26**, 107.
57 I. Fdez. Galván, M. Vacher, A. Alavi, C. Angeli, F. Aquilante, J. Autschbach, J. J. Bao, S. I. Bokarev, N. A. Bogdanov, R. K. Carlson, L. F. Chibotaru, J. Creutzberg, N. Dattani, M. G. Delcey, S. S. Dong, A. Dreuw, L. Freitag, L. M. Frutos, L. Gagliardi, F. Gendron, A. Giussani, L. González, G. Grell, M. Guo, C. E. Hoyer, M. Johansson, S. Keller, S. Knecht, G. Kovačević, E. Källman, G. Li Manni, M. Lundberg, Y. Ma, S. Mai, J. P. Malhado, P. Å. Malmqvist, P. Marquetand, S. A. Mewes, J. Norell, M. Olivucci, M. Oppel, Q. M. Phung, K. Pierloot, F. Plasser, M. Reiher, A. M. Sand, I. Schapiro, P. Sharma, C. J. Stein, L. K. Sørensen, D. G. Truhlar, M. Ugandi, L. Ungur, A. Valentini, S. Vancoillie, V. Veryazov, O. Weser, T. A. Wesołowski, P. O. Widmark, S. Wouters, A. Zech, J. P. Zobel and R. Lindh, *J. Chem. Theory Comput.*, 2019, **15**, 5925–5964.
58 F. Kossoski and M. Barbatti, *J. Chem. Theory Comput.*, 2018, **14**, 3173–3183.
59 E. Pieri, D. Lahana, A. M. Chang, C. R. Aldaz, K. C. Thompson and T. J. Martínez, *Chem. Sci.*, 2021, **12**, 7294–7307.
60 A. Dreuw and M. Head-Gordon, *Chem. Rev.*, 2005, **105**, 4009–4037.
61 L. Wang and O. V. Prezhdo, *J. Phys. Chem. Lett.*, 2014, **5**, 713–719.
62 V. Athavale, H.-H. Teh and J. Subotnik, *J. Chem. Phys.*, 2021, **15**, 154105.
63 A. Dreuw and M. Wormit, *Wiley Interdiscip. Rev.: Comput. Mol. Sci.*, 2015, **5**, 82–95.
64 D. Tuna, D. Lefrancois, Ł. Wolański, S. Gozem, I. Schapiro, T. Andruniów, A. Dreuw and M. Olivucci, *J. Chem. Theory Comput.*, 2015, **11**, 5758–5781.
65 B. O. Roos, R. Lindh, P. A. Malmqvist, V. Veryazov and P.-O. Widmark, *Multiconfigurational Quantum Chemistry*, John Wiley & Sons, 2016, pp. 157–219.
66 R. Improta and F. Santoro, *J. Phys. Chem. A*, 2005, **109**, 10058–10067.
67 W. Fuß, C. Kosmidis, W. E. Schmid and S. A. Trushin, *Chem. Phys. Lett.*, 2004, **385**, 423–430.
68 I. N. Ioffe and A. A. Granovsky, *J. Chem. Theory Comput.*, 2013, **9**, 4973–4990.
69 L. Camont, C. H. Cottart, Y. Rhayem, V. Nivet-Antoine, R. Djelidi, F. Collin, J. L. Beaudeux and D. Bonnefont-Rousselot, *Anal. Chim. Acta*, 2009, **634**, 121–128.
70 B. De Souza, G. Farias, F. Neese and R. Izsák, *J. Chem. Theory Comput.*, 2019, **15**, 1896–1904.

